Effect of Nose Bluntness and Cone Angle on Slender-Vehicle Transition

L. E. Ericsson*
Lockheed Missiles and Space Company, Inc., Sunnyvale, California

An analysis of available experimental results demonstrates that the effect of slender-cone geometry on boundary-layer transition is of inviscid origin and can be predicted by using embedded Newtonian theory. That is, the combined effect of cone half-angle and nose bluntness on transition can be simulated analytically in a way very similar to the way that the effect on slender-vehicle unsteady aerodynamics has been simulated earlier. The practical consequence for the vehicle designer is that experimental transition results for one blunted-cone geometry can be extrapolated analytically to predict what will be the effect on the transition characteristics of a change of cone half-angle and/or nose bluntness.

Nomenclature

d = body diameter
D_N = nose drag, coefficient $C_{DN} = D_N/(\rho_\infty U_\infty^2/2) \times (\pi d_N^2/4)$
k_e, k_I, k_C = proportionality constants, Eqs. (9), (A1), and (A2), respectively
ℓ = sharp cone body length
M = Mach number
p = static pressure, coefficient $C_p = (p - p_\infty)/(\rho_\infty U_\infty^2/2)$
r = body radius
Re = Reynolds number based on freestream conditions: $Re_\ell = U_\infty \ell/\nu_\infty$; $Re_s = U_\infty s/\nu_\infty$; $Re_N = U_\infty r_N/\nu_\infty$
s = distance along surface from forward stagnation point
T = temperature
U = axial velocity
x' = distance along surface from sharp cone apex
x = axial body coordinate from sharp cone apex
x_0 = start of conic frustum on blunted cone
y = height above conic frustum (see Fig. 7)
α = angle of attack (negative sign for windward side)
δ = boundary-layer thickness
Δ = difference
θ_c = cone half-angle
ν = kinematic viscosity
ρ = air density
χ = hypersonic similarity parameter (see Fig. 6)
χ_1, χ_2 = defined in Fig. 6
ϕ = turbulence propagation angle (see Fig. 7a)

Subscripts

AD = adiabatic wall
BB = blunt body
B, N = base and nose, respectively
c = conic frustum
e = edge of boundary layer
EW = entropy wake impingement
I = incompressible flow
i = inviscid flow
LB = "large" bluntness
o = $d_N = 0$
s = body surface
SB = "small" bluntness
SW = entropy swallowing
t = total
TR = transition
W = wall
∞ = freestream conditions

Presented as Paper 87-1415 at the AIAA 19th Fluid Dynamics, Plasma Dynamics, and Lasers Conference, Honolulu, HI, June 8-10, 1987; received July 23, 1987; revision received Jan. 14, 1988.

*Senior Consulting Engineer. Fellow AIAA.

Introduction

WHILE a gradual advancement of boundary-layer transition forward from the base usually is observed on slender conical re-entry bodies, it also frequently has happened, according to flight test results, that transition has moved very fast forward from the base. Morkovin[1] has catalogued the numerous possible causes of anomalous transition behavior at hypersonic speeds, many of which could result in such a transition behavior. The present paper discusses an inviscid flow mechanism that can cause transition to move forward very fast; i.e., the effect of the nose-bluntness-induced entropy gradient on the boundary-layer development.[2] Far downstream of the nose, the transition Reynolds number can be increased by up to one order of magnitude due to entropy swallowing effects. When the Reynolds number is increased so that transition starts occurring closer to the nose, entropy impingement effects greatly speed up the forward transition movement.

Analytic Approach

Far downstream from the nose, the gradual advancement forward of transition with increasing Reynolds number is delayed by the nose-bluntness-generated low-velocity/high-entropy shear layer over the conic frustum.[3,4] How transition is dominated by this entropy swallowing phenomenon has been shown by Softley et al.[5] (see Fig. 1). It was shown in Ref. 6 that the inviscid flow parameter x_{EWi}, defined as the location where the blunted-cone pressure has reached the sharp-cone level, could be used as the correlation parameter as well as the viscous entropy swallowing parameter x_{SW} used in Ref. 5 (compare Figs. 1 and 2). The present paper is a follow-up of Ref. 6 and discusses how this transition dependence on the nose-bluntness-induced inviscid shear layer changes when moving from the entropy swallowing (small bluntness) to the entropy impingement (large bluntness) region.

Softley[5,7] has shown that the transition movement forward with increasing Reynolds number is greatly speeded up when transition occurs upstream of completed entropy swallowing (see Fig. 3). The reason for this difference in transition behavior for "large" and "small" nose bluntness is revealed by Cleary's theoretical and experimental investigations of the shock layer on a 15-deg blunted cone[8-10] (see Fig. 4). (The quotation marks are used to warn the reader that large and small nose bluntness here means small and very small in the terminology applied to unsteady aerodynamics, as will be shown later.)

Far downstream from the nose, at $x/x_{EWi} = 4.10$ ($x/r_N = 46.76$), the entropy layer has been swallowed completely by the boundary layer, evidenced by the experimentally measured uniform entropy layer. At $x/x_{EWi} = 0.75$ ($x/r_N = 6.26$), on the other hand, the experimental data show the theoretically predicted high-entropy shear. The presence of external flow shear is promoting transition, as it generates turbulence.[11,12] Comparing the total pressure profiles in Fig. 4 for $x/r_N = 6.26$ and $x/r_N = 17.56$, one can visualize the inflexional inviscid instability discussed by Stetson et al.[13]

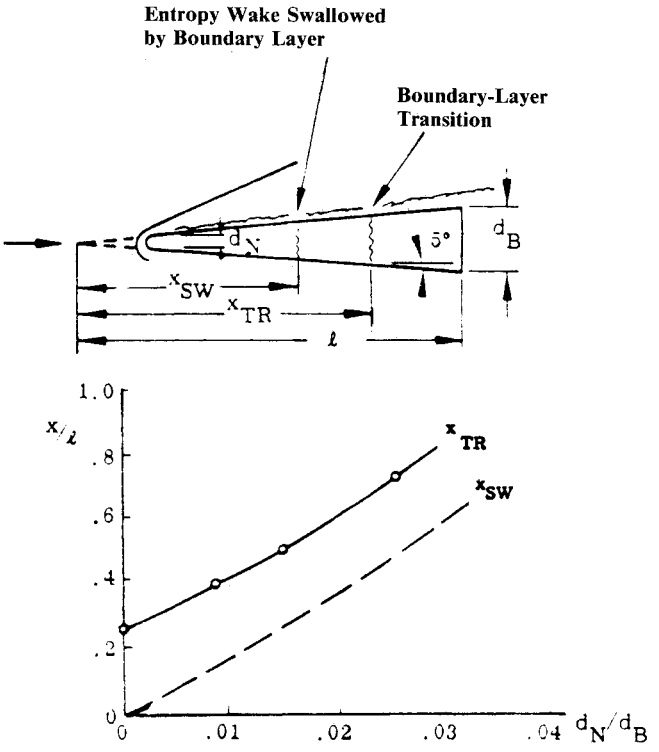

Fig. 1 Effect of entropy swallowing on boundary-layer transition on a slender cone.[5]

Analysis

The inviscid scaling parameter x_{EWi}, shown in Fig. 2, is for hypersonic flow conditions obtained as follows:[6]

$$x_{EWi}/r_N = (1 + 2\chi_1 C_{DN}^{1/2}\theta_c^{-1})/\theta_c \tag{1}$$

where χ_1 is obtained by using the linear expression for the blunted-cone dynamic pressure ratio in Ref. 14 when defining the value $\chi_1 = 0.6$, for which the sharp-cone pressure level $\rho U^2/\rho_\infty U_\infty^2 = 1$ is first reached.

It was shown in Ref. 6 that the experimental transition results for "small" nose bluntness obeyed the following simple relationship (see Fig. 2):

$$x_{TR} = x_{TRo} + x_{EWi} + \Delta x_{TR} \tag{2}$$

or

$$x_T/x_{EWi} = 1 + \Delta x_{TR}/x_{EWi} + x_{TRo}/x_{EWi} \tag{3}$$

In Fig. 5, experimental transition results[7,15-18] are plotted using x_{EWi} as indicated in Eq. (3). As can be seen, the "entropy impingement distance" x_{EWi} is a good scaling parameter, not only for "small" but also for "large" nose bluntness. As nose bluntness is increased, the blunt-body limit $x_T/x_{TRo} = 1.8$ is approached. Using the embedded Newtonian theory,[14,19] the entropy shear region, where the large-nose bluntness behavior is expected, can be defined as $\chi_2 \le \chi \le \chi_1$ (see Fig. 6). It is shown in Fig. 3 of Ref. 19 that Method of Characteristics computations give $\chi_2 \approx 0.07$ for hypersonic flow conditions $M_\infty\theta_c > 1$, $M_\infty \gg 1$. The blunt-body behavior is restricted to $x < x_{BB}$, where x_{BB} is given by Eq. (1) when substituting χ_1 with χ_2. Using this new equation together with Eq. (1), the latter defining x_{EW}, one obtains

$$\frac{x_{BB}}{x_{EWi}} = \frac{1 + 2\chi_2 C_{DN}^{1/2}\theta_c^{-1}}{1 + 2\chi_1 C_{DN}^{1/2}\theta_c^{-1}} \tag{4}$$

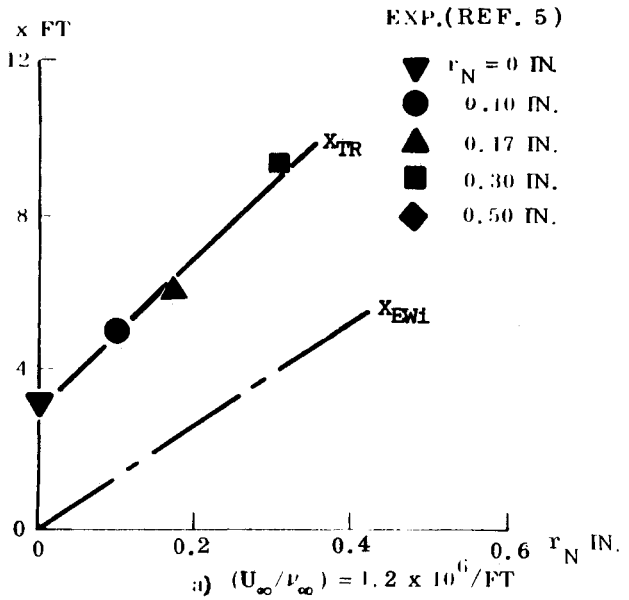

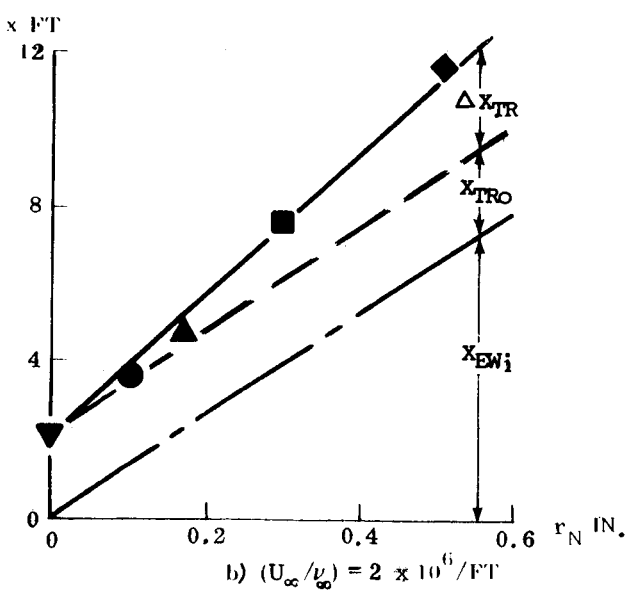

Fig. 2 Transition length on 5-deg cones with different nose radii.

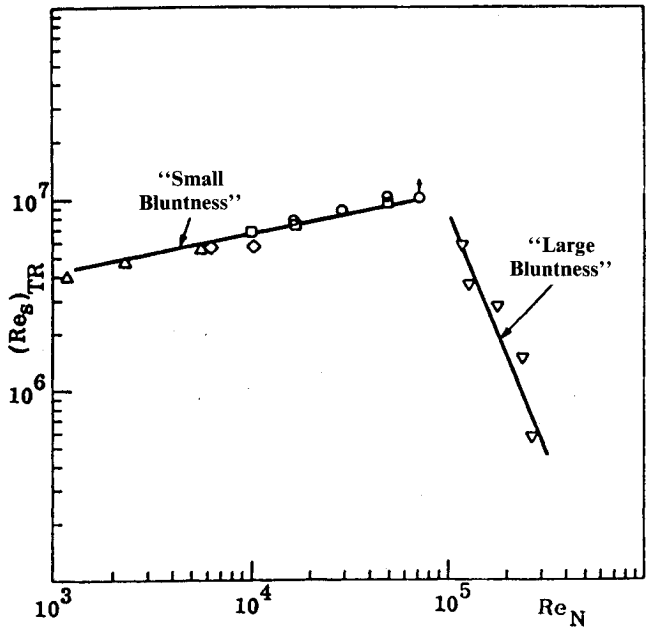

Fig. 3 Transition Reynolds number for blunted slender cones.[5]

For $\theta_c = 5$ and 8 deg, Eq. (4) gives $x_{BB}/x_{EWi} = 0.18$ and 0.21, respectively. These values are in good agreement with the experimental data trend in Fig. 5. At $M_\infty < 10$, Eq. (1) is modified by Mach number effects.[19]

For the wind tunnel test results,[7,15-18] the parameter x_{TR}/x_{EWi} in Eq. (3) appears to be in the range of $0.1 < \Delta x_{TR}/x_{EWi} < 0.9$, whereas for the flight test data, the range is $1.6 < \Delta x_{TR}/x_{EWi} < 2.3$. The value 1.6 for the predicted minimum nose radius is well defined (see Fig. 5). However, the value 2.3 for the maximum predicted nose radius is more uncertain since it is based upon only one data point[20] (see Fig. 5).

The results in Fig. 5 are interesting in many respects. The correlation of the "small" nose bluntness data was demonstrated in Ref. 6. The difference in the $\Delta x_{TR}/x_{EWi}$ values represents mainly the influence of the freestream turbulence level, with transition occurring earlier in the noisy wind tunnels[20] than in free flight. The correlation of the "large" nose bluntness data could also be expected based upon the results in Ref. 14, where it was shown that the large effect of nose bluntness on slender-cone unsteady aerodynamics, determined by inviscid theory, could be compared directly with experimental (viscous flow) results. The reason for this is that viscous crossflow effects, including those caused by support interference,[21] are essentially the same for the sharp and the blunted cones. Consequently, the ratio between blunted- and slender-cone

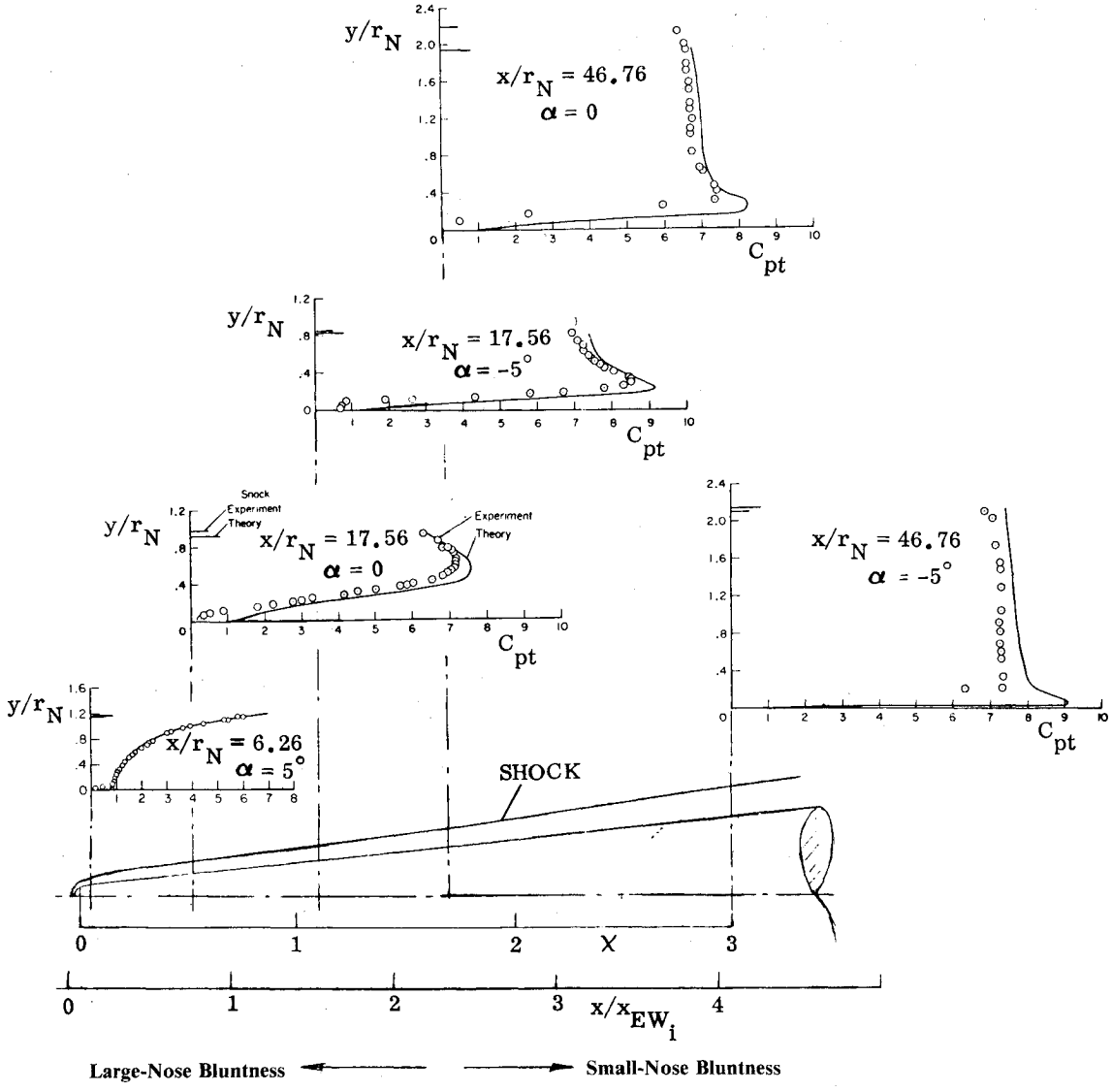

Fig. 4 Theoretical and experimental shock layer pitot pressure profiles on a 15-deg blunted cone at $M_\infty = 10.6$.[10]

stability derivatives is the same in viscous and inviscid flow within the experimental accuracy of dynamic tests, ± 10%. As a matter of fact, the difference between experimental results obtained in different ground facilities is larger than the error due to the assumption of similarity in viscous flow effects.[22]

Apparently, the effect of the nose-bluntness-induced inviscid flow vorticity on transition is so large that it completely overpowers the freestream turbulence effects in the "large" nose bluntness region, judging by the collapse of the experimental transition results shown in Fig. 5. (That flight data in the "large" nose bluntness region were indeed obtained is confirmed by the observed windward side transition forward of leeward side transition.[6,23]) This is only true well within the "large" nose bluntness region. The upper boundary of this region is strongly affected by freestream turbulence, determining the value of $\Delta x_{TR}/x_{EWi}$. The lower boundary is the blunt-body limit, as was discussed earlier. The results in Fig. 5 give the following definition of the "large" nose bluntness effect on transition, provided that $x_{BB}/x_{EWi} < x_{TRo}/x_{EWi} < (x_{TRo}/x_{EWi})_{SB}$:

$$(x_{TR}/x_{EWi})_{LB} = 1.8\,(x_{BB}/x_{EWi}) + 4.75\,[(x_{TR}/x_{EWi}) - (x_{BB}/x_{EWi})] \tag{5}$$

The upper limit $(x_{TRo}/x_{EWi})_{SB}$ decreases from approximately unity for the flight data to roughly half that value for the noisiest wind tunnel data (Fig. 5). The term x_{BB}/x_{EWi} is given by Eq. (4).

The "large" nose bluntness region extends far beyond $x_{TR}/x_{EWi} = 1$ because in hypersonic flow transition occurs through the spreading of turbulence (induced by the entropy shear in the present case) from the boundary-layer edge[24-26] (see Fig. 7a). Transition at the surface occurs 50–100 boundary-layer thicknesses downstream of the disturbance at the boundary-layer edge ($\phi_W = 0.5$–1.0 deg for $M_e = 2.5$–13.6).[26] For the 2.87-deg cone in Ref. 26 (with $r_N = 0.01$ cm), this x_{eTR} range stretches from $x_{eTR}/x_{EWi} = 9$ to $x_{TR}/x_{EWi} = 17.5$–26.0.

It is shown in the Appendix that when x_{TR}/x_{EWi} is moved forward from 9 to 1, the (x_{TR}/x_{EWi}) range is moved forward from 17.5–26.0 to 1.8–2.7 for adiabatic wall and to 2.1–3.2 for cold wall conditions. These values are in rather good agreement with the results shown in Fig. 5. The cold wall results should apply to the flight data and the adiabatic wall results to the wind tunnel data.

The critical nose bluntness value, above which the blunted cone will have the "rushing" transition behavior, is given by Eq. (1) as follows:

$$x_{EWi}/r_N = (1 + 2\chi_1\, C_{DN}^{1/2}\theta_c^{-1})/\theta_c \tag{6a}$$

$$(x_{TR}/x_{EWi})_{\text{crit}} = \ell/x_{EWi} \tag{6b}$$

With $r_B/\ell = \theta_c$, one obtains

$$(r_N/r_B)_{\text{crit}} = [(x_{TR}/x_{EWi})_{\text{crit}}\,(1 + 2\chi_1\, C_{DN}^{1/2}\theta_c^{-1})]^{-1} \tag{7}$$

Figure 5 gives $(x_{TR}/x_{EWi})_{\text{crit}} = 2.00 \pm 0.25$ for the ground tests. With $C_{DN} = 0.9$ for a hemispherical nose tip, one obtains for $\theta_c = 0.1$ (5.7 deg) the following critical nose bluntness ratio at hypersonic conditions ($\chi_1 = 0.6$):

$$(r_N/r_B)_{\text{crit}} = 0.04 \pm 0.005$$

That is, large nose bluntness in regard to transition behavior is very much smaller than large nose bluntness as thought of in regard to vehicle aerodynamics.[14]

The relative insensitivity to Mach number of the "small" nose bluntness transition data in Fig. 5 is a surprise. It is true that x_{EWi} incorporates the effect of Mach number. However, for x_{TR}/x_{EWi} to be independent of Mach number, it is also required that x_{TR}/x_{eTR} be insensitive to Mach number. Why this may be true in an approximate sense can be explained as follows

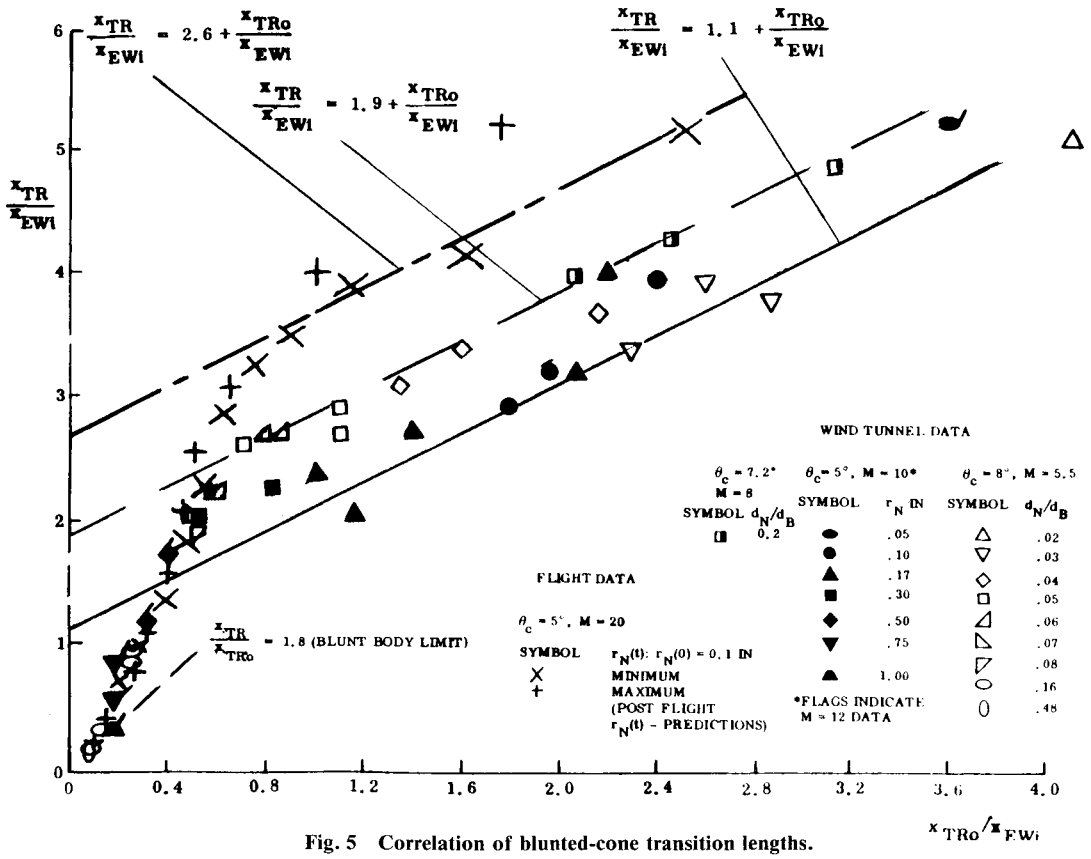

Fig. 5 Correlation of blunted-cone transition lengths.

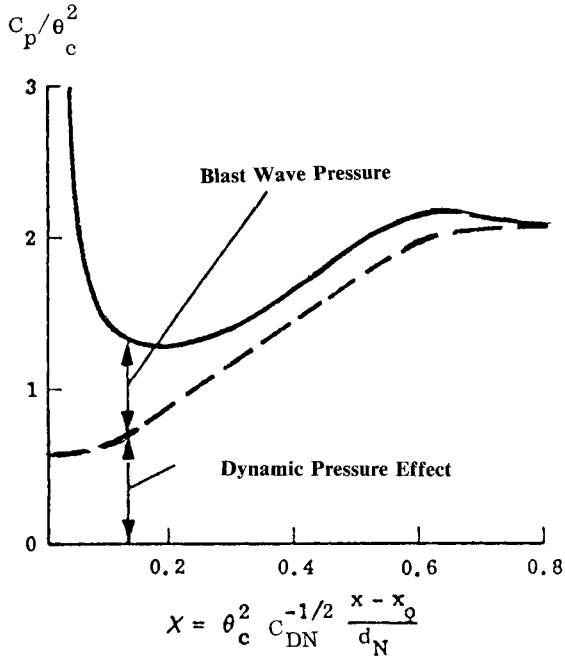

a) C_p/θ_c^2 vs χ

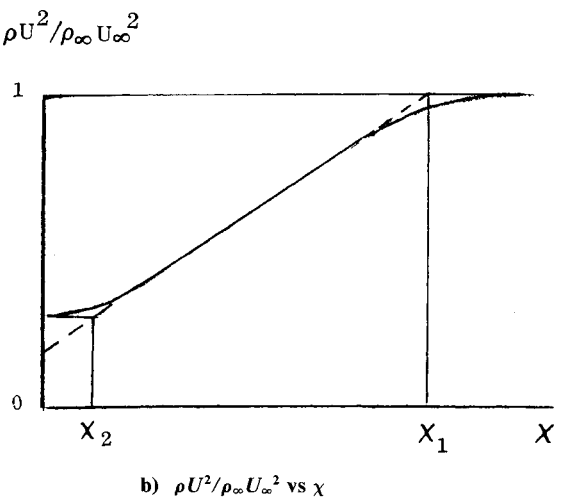

b) $\rho U^2/\rho_\infty U_\infty^2$ vs χ

Fig. 6 Static pressure correlation on blunted slender cones.

(see Fig. 7b):

$$x_{TR} = x_{eTR} + \Delta x'_{eTR} \cos\theta_c \tag{8a}$$

$$\Delta x'_{eTR} = 0.95\delta \cot\phi_W \tag{8b}$$

For slender cones, e.g., $\theta_c < 10$ deg, Eq. (8) and Ref. 26 give

$$x_{TR} = x_{eTR} + k_e \delta_{eTR} \tag{9a}$$

$$k_e = 55 - 110 \text{ for } 2.5 < M_e < 13.6 \tag{9b}$$

For transition far downstream of the nose, e.g., $x_{TR}/x_{EWi} > 2$ in Fig. 5, the boundary-layer edge conditions at transition are approximately the same as for a sharp cone. Consequently, the following approximation can be made:

Sharp cone:

$$\delta_{eTRo}/(x_{eTRo})^{1/2} \sim (\nu_e/U_e)^{1/2} \tag{10a}$$

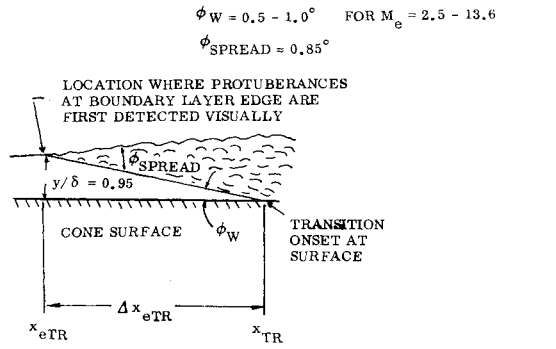

a. Growth of turbulence in a hypersonic boundary layer (Ref. 26)

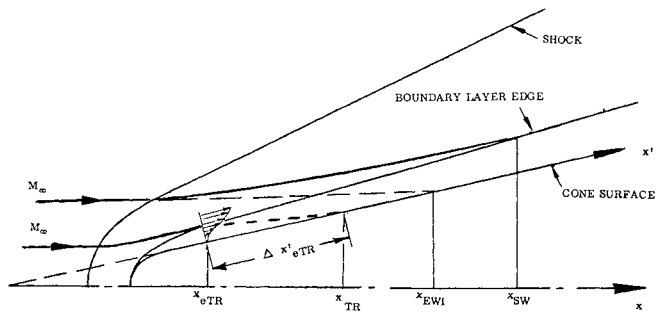

b. Definition of "entropy wake" effects

Fig. 7 Hypersonic transition mechanism.

Blunted cone:

$$\delta_{eTR}/(x_{eTR})^{1/2} \sim (\nu_e/U_e)^{1/2} \tag{10b}$$

That is, the boundary-layer thickness at transition is determined by the distance from the nose, regardless of nose bluntness.

It is well known that transition Reynolds number increases with Mach number.[27] If the boundary-layer thickness squared were to increase with M_e at the same rate as the transition Reynolds number, the ratio $\delta_{eTR}/(x_{eTR})^{1/2}$ would remain constant, which in turn implies that the ratio x_{TR}/x_{eTR} would be insensitive to Mach number, in agreement with the experimental data trends in Fig. 5. Figure 8 shows that this postulated condition is indeed in general agreement with the facts; the cold wall and adiabatic wall growth rates for $[\delta(M_e)/\delta(0)]^2$ follow the experimentally observed Re_{xTR} variations with boundary-layer edge Mach number. No additional Mach number effect can be distinguished above the data scatter. That is, the (x_{TR}/x_{EWi}) values are more sensitive to the variations in ambient disturbance levels between tests than to differences in Mach number. When comparing Figs. 5 and 8, it is obvious that the difficulty in predicting blunted-cone transition is not the determination of the effect of nose bluntness.

Using the values $\chi_1 = 0.6$ and $\chi_2 = 0.07$, the nose bluntness and cone angle regions for the different types of entropy effects shown in Fig. 9 are obtained. The results are for the adiabatic wall conditions applicable to ground facility tests. The boundaries would be slightly different for the cold wall conditions representative of full-scale flight. Figure 9 shows that a great number of re-entry vehicles will experience the full-entropy gradient effect described by Eq. (5). Selecting the critical nose bluntness defined by $\chi = \chi_1$ in Fig. 9 would give the minimum transition altitude for a re-entering slender cone. It is interesting to note that many of the re-entry vehicles for which unusually low transition altitudes have been recorded have nose bluntnesses falling in the shaded region around $\chi = \chi_1$ in Fig. 9. Equally interesting to note is that most blunted cones fall in the region of full-entropy gradient and should, therefore, experience the fast forward movement of transition for increas-

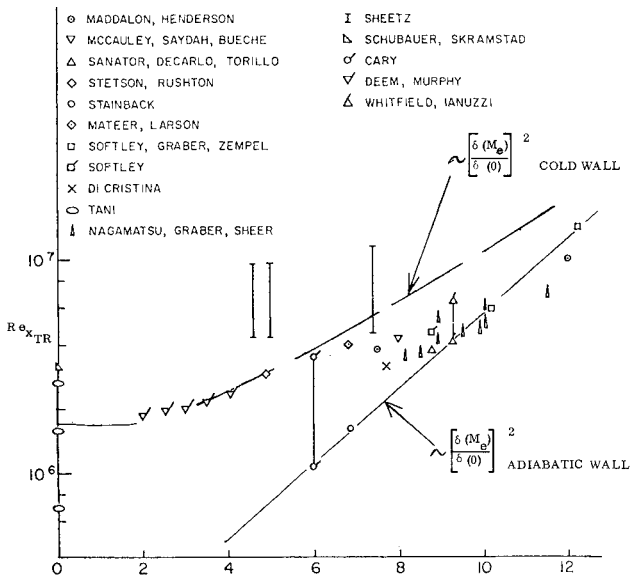

Fig. 8 Sharp-cone transition Reynolds number as a function of Mach number.[27]

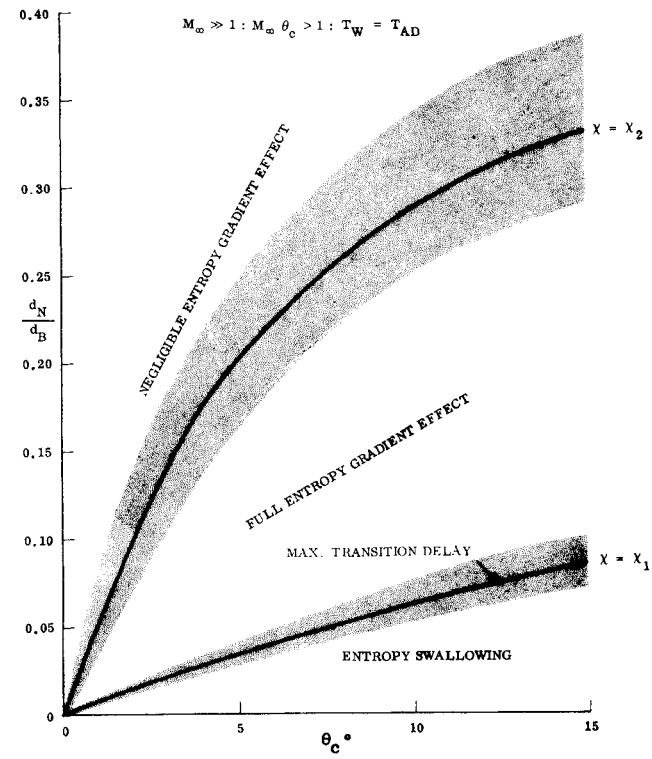

Fig. 9 Bluntness and cone angle combinations giving different entropy wake effects on hypersonic slender cone transition.

ing Reynolds number, i.e., for decreasing altitude of a re-entry vehicle. This is also in general agreement with flight experience.

In view of the many flow mechanisms through which transition at hypersonic speeds can take place,[1] the present analysis can be of great help as it can eliminate the (inviscid) effect of nose bluntness from the experimental results. The analysis makes it possible to extrapolate to obtain the sharp cone transition length x_{TRo} corresponding to the measured blunted cone transition length x_{TR} (see Fig. 5). In this manner, the viscous flow effects on transition, such as ablation-induced roughness, can be extracted. In regard to mass-addition effects on transition, however, one has first to determine the blowing-induced change of the bowshock with associated effect on the entropy wake[28] before the viscous blowing effects can be isolated.

Conclusions

An analysis of available experimental transition data for slender blunted cones has shown the following:

1) Both large and small nose bluntness transition data can be correlated using the length (x_{EWi}) of the entropy wake as the characteristic length for the inviscid bluntness effect. (Sharp cone pressure is first reached at $x = x_{EWi}$).

2) The complete entropy swallowing of the boundary layer occurring for small nose bluntness causes a delay of transition ($\Delta x_{TR}/x_{EWi}$) that is attenuated by wind tunnel noise and reaches its maximum in free flight, where an order of magnitude increase of the transition Reynolds number is possible for the optimum nose bluntness.

3) At larger nose bluntnesses, the forward movement of transition with increasing Reynolds number is speeded up greatly by entropy impingement effects.

The intrinsic value of the presented analysis is that it provides the means for extrapolation from transition results for one blunted-cone geometry to another with different cone angle and/or nose bluntness, including the sharp-cone geometry.

Appendix: Estimate of Blunted-Cone Boundary-Layer Thickness

When determining the boundary-layer thickness at $x_{eTR} = x_{EWi}$, one can neglect the nose tip geometry and select the sharp-cone apex as the start of the wetted cone area. Equation (1) gives $x_{EWi}/r_N = 124$ for $\theta_c = 0.1$ (5.7 deg). For slender cones, one can also neglect the difference between x' and x (Fig. 7b). The boundary-layer thickness at $x = x^*$ will be determined. In the real viscous flow, $x^* = x_{SW}$. For the inviscid flow case $x^* = x_{EWi}$ is used as a reference. In incompressible flow, the laminar boundary-layer thickness at $x = x^*$ is

$$\delta(0) = \int_0^{x^*} \frac{d\delta_I}{dx}\, dx = k_I x^{*1/2} \tag{A1}$$

The boundary-layer thickness at constant $M_e > 1.0$ can be written as follows:

$$\delta(M_e) = \delta(0)\,[1 + k_C M_e^2] \tag{A2}$$

Thus, at $x = x^*$,

$$\delta(M_e) = \int_0^{x^*} \frac{d\delta_I}{dx}\,[1 + k_C M_e^2]\, dx \tag{A3}$$

It has been found[4,15] that the boundary-layer edge Mach number varies almost linearly between the sonic portion on the nose tip and the sharp-cone value downstream on the frustum. Thus,

$$M_e = 1 + [(M_c - 1)/x^*]x \tag{A4}$$

(For the present case[26] with $M_c = 13.6$, this approximation, Eq. (A4), gives less than 10% error.) Combining Eqs. (A1), (A3), and (A4) gives

$$\delta(M_e) = \delta(0) + k_C \int_0^{x^*} \left(\frac{k_I}{2}\right) x^{-1/2} \left[1 + \left(\frac{M_c - 1}{x^*}\right)x\right]^2 dx \tag{A5}$$

or

$$\frac{\delta(M_c)}{\delta(0)} = 1 + k_C \left[1 + \frac{2(M_c - 1)}{3} + \frac{(M_c - 1)^2}{5}\right] \tag{A6}$$

The constant k_C has the following value:

$$k_C = \begin{cases} 0.02 : T_W = T_e \\ 0.05 : T_W = T_{AD} \end{cases} \tag{A7}$$

Thus, with $M_c = 13.6$,[26] Eq. (A6) gives

$$\frac{\delta(M_e)}{\delta(0)} = \begin{cases} 1.82 : T_W = T_e \\ 3.05 : T_W = T_{AD} \end{cases} \tag{A8}$$

Far downstream at $x_{eTR}/x_{EWi} = 9$,

$$\frac{\delta(M_c)}{\delta(0)} = 1 + k_C M_c^2 = \begin{cases} 4.40 : T_W = T_e \\ 10.35 : T_W = T_{AD} \end{cases} \tag{A9}$$

That is,

$$\frac{\delta(M_e)}{\delta(0)} = \begin{cases} 1.82 : T_W = T_e \\ 3.05 : T_W = T_{AD} \end{cases} \tag{A10}$$

and the values corresponding to $x_{eTR}/x_{EWi} = 9$ and $x_{TR}/x_{EWi} = 17.5\text{–}26.0$ are

$$\frac{x_{eTR}}{x_{EWi}} = 1 \tag{A11a}$$

$$\frac{x_{TR}}{x_{EWi}} = \begin{cases} 2.1\text{–}3.2 : T_W = T_e \\ 1.8\text{–}2.7 : T_W = T_{AD} \end{cases} \tag{A11b}$$

References

[1]Morkovin, M. V., "Critical Evaluation of Transition from Laminar to Turbulent Shear Layers with Emphasis on Hypersonically Traveling Bodies," Flight Dynamics Lab., Wright-Patterson Air Force Base, Dayton, OH, AFFDL-TR-68-149, March 1969.

[2]Ericsson, L. E., "Unsteady Aerodynamics of an Ablating Flared Body of Revolution Including Effects of Entropy Gradient," *AIAA Journal,* Vol. 6, Dec. 1968, pp. 2395–2401.

[3]Ferri, A. and Libby, P. A., "Note on an Interaction Between the Boundary Layer and the Inviscid Flow," *Journal of the Aeronautical Sciences,* Vol. 21, Feb. 1954, p. 130.

[4]Zakkay, V. and Krause, E., "Boundary Conditions at the Outer Edge of the Boundary Layer on Blunted Conical Bodies," *AIAA Journal,* Vol. 1, July 1963, pp. 1671–1672.

[5]Softley, E. J., Graber, B. C., and Zempel, R. C., "Experimental Observation of Transition of the Hypersonic Boundary Layer," *AIAA Journal,* Vol. 7, Feb. 1969, pp. 257–263.

[6]Ericsson, L. E., "Correlation of Attitude Effects on Slender Vehicle Transition," *AIAA Journal,* Vol. 12, April 1974, pp. 523–529.

[7]Softley, E. J., "Transition of the Hypersonic Boundary Layer on a Cone: Part II—Experiments at $M = 10$ and More on Blunt Cone Transition," General Electric Space Sciences Lab., Missile and Space Division, Valley Forge, PA, Rept. R68SD14, Oct. 1968.

[8]Cleary, J. W., "Effects of Angle of Attack and Nose Bluntness on the Hypersonic Flow Over Cones," AIAA Paper 66-414, June 1966.

[9]Cleary, J. W., "An Experimental and Theoretical Investigation of the Pressure Distribution and Flow Fields of Blunted Cones at Hypersonic Mach Numbers," NASA TND-2969, Aug. 1965.

[10]Cleary, J. W., "Effects of Angle of Attack and Bluntness on the Shock-Layer Properties of a 15° Cone at a Mach Number of 10.6," NASA TND-4909, Nov. 1968.

[11]Davis, R. T. and Flugge-Lotz, I., "The Laminar Compressible Boundary-Layer in the Stagnation Point Region of an Axisymmetric Blunt Body Including the Second-Order Effect of Vorticity Interaction," *International Journal of Heat and Mass Transfer,* Vol. 7, 1964, pp. 341–370.

[12]Deissler, R. G., "Growth of Turbulence in the Presence of Shear," *The Physics of Fluids,* Vol. 5, Nov. 1972, pp. 1918–1920.

[13]Stetson, K. F., Thompson, E. R., Donaldson, J. C., and Siler, L. G., "Laminar Boundary Layer Stability Experiments on a Cone at Mach 8, Part 2: Blunt Cone," AIAA Paper 84-0006, Jan. 1984.

[14]Ericsson, L. E., "Unsteady Embedded Newtonian Flow," *Astronautica Acta,* Vol. 18, 1973, pp. 309–330.

[15]Stetson, K. F. and Rushton, G. H., "A Shock Tunnel Investigation of the Effects of Nose Bluntness, Angle of Attack, and Boundary Layer Cooling on Boundary Layer Transition at a Mach Number of 5.15," *AIAA Journal,* Vol. 5, May 1967, pp. 899–906.

[16]Muir, J. F. and Trujillo, A. A., "Experimental Investigation of the Effects of Nose Bluntness, Free-Stream Unit Reynolds Number, and Angle of Attack on Cone Boundary Layer Transition at a Mach Number of 6," AIAA Paper 72-216, Jan. 1972.

[17]Martellucci, A., "Asymmetric Transition Effects on the Static Stability and Motion History of a Slender Vehicle," Aerospace Corp., San Bernadino, CA, SAMSO TR-70-141, 1970.

[18]Martellucci, A., Maguire, B. L., and Neff, R. S., "Analysis of Flight Test Transition and Turbulent Heating Data. Part I—Boundary Layer Transition Results," NASA CR-129045, Nov. 1972.

[19]Ericsson, L. E., "Generalized Unsteady Embedded Newtonian Flow," *Journal of Spacecraft and Rockets,* Vol. 12, Dec. 1975, pp. 718–726.

[20]Pate, S. R., "Dominance of Radiated Aerodynamic Noise on Boundary Layer Transition in Supersonic-Hypersonic Wind Tunnels, Theory and Application," Arnold Engineering Development Center, Tullahoma, TN, AEDC-TR-77-107, March 1978.

[21]Ericsson, L. E. and Reding, J. P., "Review of Support Interference in Dynamic Tests," *AIAA Journal,* Vol. 21, Dec. 1983, pp. 1652–1666.

[22]Ericsson, L. E., "Parametric Investigations of Slender Cone Nose Bluntness Effects," *Journal of Spacecraft and Rockets,* Vol. 23, Jan.–Feb. 1986, pp. 126–128.

[23]Ericsson, L. E., "Transition Effects on Slender Vehicle Stability and Trim Characteristics," AIAA Paper 73-216, Jan. 1973.

[24]Maddalon, D. V. and Henderson, A. Jr., "Boundary-Layer Transition on Sharp Cones at Hypersonic Mach Numbers," *AIAA Journal,* Vol. 6, March 1968, pp. 424–431.

[25]Owen, F. K., "Fluctuations and Transition Measurements in Compressible Boundary Layers," AIAA Paper 70-745, 1970.

[26]Fisher, M. C. and Weinstein, L. M., "Cone Transitional Boundary-Layer Structure at $M_e = 14$," *AIAA Journal,* Vol. 10, May 1972, pp. 699–701.

[27]Donaldson, C. dy P., Sullivan, R. D., and Yates, J. E., "An Attempt to Construct an Analytical Model of the Start of Compressible Transition," Flight Dynamics Lab., Wright-Patterson Air Force Base, Dayton, OH, AFFDL-TR-70-153, Jan. 1971.

[28]Ericsson, L. E. and Guenther, R. A., "Dynamic Instability Caused by Forebody Blowing," *AIAA Journal,* Vol. 11, Feb. 1973, pp. 231–233.